

PSFC/JA-00-31

**Identification of Mercier Instabilities in
Alcator C-Mod Tokamak**

Y. In, J.J. Ramos, R.J. Hastie, P.J. Catto, A.E. Hubbard, I.H. Hutchinson,
E. Marmor, M. Porkolab, J. Snipes, S. Wolfe, G. Taylor¹, A. Bondeson²

September 2000

Plasma Science and Fusion Center
Massachusetts Institute of Technology
Cambridge, MA 02139 USA

¹Princeton Plasma Physics Laboratory, Princeton, NJ 08543

²Chalmers University of Technology, Goteborg, Sweden.

This work was supported by the U.S. Department of Energy, Cooperative Grant No. DE-FC02-99ER54512. Reproduction, translation, publication, use and disposal, in whole or in part, by or for the United States government is permitted.

Submitted for publication to *Physics of Plasmas*.

September 28, 2000

Identification of Mercier instabilities in Alcator C-Mod tokamak

Y. In, J. J. Ramos, R. J. Hastie, P. J. Catto,
A. E. Hubbard, I. H. Hutchinson, E. Marmor, M. Porkolab,
J. Snipes, S. Wolfe, G. Taylor[†], A. Bondeson[‡]

MIT Plasma Science and Fusion Center, Cambridge, MA 02139

[†] Princeton Plasma Physics Laboratory, Princeton, NJ 08543

[‡] Chalmers University of Technology, Göteborg, Sweden

During current ramp-up discharges, highly localized magnetohydrodynamic (MHD) fluctuations were observed on the electron cyclotron emission (ECE) diagnostics of Alcator C-Mod tokamak [I. H. Hutchinson *et al.*, Phys. Plasmas **1**, 1511 (1994)]. The electron temperature profile was hollow, while the density profile was weakly decreasing. Assuming that the equilibration time was short enough to quickly thermalize ions the pressure profile was also found to be hollow. Using this pressure profile as an additional constraint to the EFIT program, an equilibrium with reversed shear was constructed having a $q(0) \gg 1$. The localized MHD activity was observed near the inner $q=5$ rational surface in this reconstructed equilibrium, where the Mercier criterion for ideal MHD stability was violated because of the reversed pressure gradient ($dp/dr > 0$), $q > 1$ and moderate shear. When kinetic effects were added, the ideal Mercier mode was finite ion Larmor radius (FLR) stabilized. However, ion Landau damping was found to be strong enough to drive a kinetic Mercier instability.

PACS Number:52.35.Py, 52.35.Qz, 52.55.Fa

I. Introduction

During the current ramp-up phase of some discharges in the 1999 run campaign, highly localized magnetohydrodynamic (MHD) fluctuations were observed on the electron cyclotron emission (ECE) diagnostics of Alcator C-Mod.¹ The detailed analysis presented here shows that these fluctuations can be attributed to a modified Mercier² instability. We believe that no experimental identification of Mercier instability in tokamaks has been previously reported, though there have been many theoretical speculations regarding Mercier instability in other toroidal devices.^{3,4} Recent theoretical studies of Mercier stability in reversed shear equilibria with monotonic pressure profiles have concluded that such equilibria are stable.⁵⁻⁷ However, during the current rise in Alcator C-Mod, reversed shear is often accompanied by hollow pressure profiles, because the current rise time is much faster than the current diffusion time, leading to an off-axis peak in the Joule heating. Under these conditions, the Mercier criterion can be violated and it is of interest to investigate such discharges for signs of a Mercier instability. One reason such instabilities are difficult to observe is that a weak Mercier mode may be stabilized by the so called finite ion Larmor radius (FLR) effect. The theory of FLR stabilization of ideal MHD modes has been developed over many years.⁸⁻¹¹ For MHD modes, Roberts and Taylor⁸ derived the FLR term from the stress tensor. Ara *et al.*⁹ investigated FLR effects on internal kink modes. Connor *et al.*¹⁰ showed that, in high- β plasmas, the calculation of FLR effects on the Mercier instability at high toroidal mode number n requires a solution of the ballooning equation. Tang *et al.*¹¹ investigated the FLR stabilization of ideal ballooning modes. Nevertheless, FLR theory is incomplete in the sense that, when stabilization is predicted, it finds a pair of purely oscillatory modes. These modes are sensitive to any additional collisional dissipation or Landau resonance in the plasma, which normally leads to destabilization of one of the oscillatory modes and damping of the other. In the cases we shall discuss here, ion Landau damping or resistivity are the non-ideal effects that drive a kinetic Mercier instability.

Before the observed localized MHD event, the electron temperature profile is observed to be hollow with an off-axis peak of around 0.9 keV. Equilibrium reconstructions using EFIT¹² indicate that the profile of the safety factor,

$q(r)$, is also non-monotonic, with the axial value, $q(0) \gg 1$, and an off-axis minimum at $r/a \sim 0.6 - 0.8$. Such features were observed in several discharges. As we will see, detailed analysis revealed that the localized MHD mode may be attributed to a FLR modified Mercier instability. In addition, these reversed shear (RS) discharges displayed global MHD activity, such as off-axis sawtooth-like events in which a fast thermal collapse was observed on some ECE channels and temperature increase on others (i.e outside of an inversion radius). An interpretation and discussion of these global fluctuations in terms of double tearing instabilities has been given by Y. In *et al.*¹³ and Z. Chang *et al.*¹⁴

In Sec. II the experimental observations of the localized MHD activity will be described. In Sec. III we will give an account of the theoretical analysis of the localized fluctuations and their identification as kinetic Mercier instabilities. Specifically, in Sec. III. A a reconstructed equilibrium, immediately prior to the MHD activity, will be discussed. In Sec. III. B we present the results of ideal MHD stability calculations, both with the MARS code¹⁵ and a quasi 1-D model. These predict Mercier instability. In Sec. III. C, we discuss finite ion Larmor radius (FLR) stabilization and show that the ideal Mercier modes found in Sec. III. B are FLR stabilized. The dominant dissipative effect for these modes is then identified as ion Landau damping, and in Sec. III. D solutions of a kinetic dispersion relation, which includes ion Landau damping, are presented. These results show that a kinetic Mercier mode is indeed predicted to be unstable in the reversed shear core of C-Mod. Sec. IV discusses the consequences of uncertainties in the ion temperature profile, while Sec. V presents a summary.

II. Experimental observation

A. Diagnostics

Alcator C-Mod is a high field ($B_T = 5\sim 8$ T), compact ($R = 0.67$ m major radius, $a = 0.22$ m minor radius), diverted tokamak. Poloidal magnetic field pickup loops have been upgraded to measure fluctuations, which can be digitized at a rate of 1 or 2 MHz. For fluctuation studies, there are six sets of toroidally displaced coils located on outboard limiters. Using the

magnetic data, the toroidal mode number(n) is usually determined unequivocally. For electron temperature measurements, two grating polychromators (GPC and GPC2) are used for this analysis. Since 1994, GPC (9 channel) has been used as a routine temperature diagnostic in C-Mod, while GPC2 (19 channel) from Princeton Plasma Physics Laboratory (PPPL) has been operational since 1998. For the purpose of observing MHD activity on electron temperature measurements, the GPC was chosen as the main diagnostic because it provides good spatial resolution (~ 1 cm) and temporal response (up to $2 \mu\text{sec}$). Its routine sampling frequency is 20 kHz. GPC2 can sample the data at slow (~ 5 kHz) and fast (~ 50 kHz) frequencies simultaneously. Thus, the slow channels are usually useful for determining the temperature profile, while the fast ones detect temperature fluctuations. As a result, if the fluctuation frequency is above the Nyquist frequency (~ 2.5 kHz) of the slow channel, it can be observed only on the fast channels of GPC2. However, the signal-to-noise ratios of the fast GPC2 channels are lower than those of GPC. As Thomson scattering density data points are sparse in time and space, the plasma density (n_e) profile is usually inferred from Abel-inverted visible Bremsstrahlung from a multichord diagnostic whose view is horizontal and near the midplane. In 1999, the visible Bremsstrahlung diagnostic was upgraded to have a high radial resolution ($\pm 2\text{mm}$), with a relative radial position uncertainty within $\pm 0.3\text{mm}$. As the brightness of the visible Bremsstrahlung diagnostic is a function of Z_{eff} , n_e , and T_e , the density can be inferred using the electron temperatures (T_e) from the ECE diagnostics, assuming the effective charge number Z_{eff} is constant.

B. Observation of localized MHD fluctuations

As shown in Fig. 1, a localized electron temperature fluctuation was observed on Channel 2 ($R = 0.716\text{m}$) of the GPC in the core. It started to grow at $t=115$ msec and lasted 10 – 15 milliseconds, moving inward (i.e. Ch 2 to Ch 1). Sawtooth-like crashes followed much later (the first normal sawtooth crash of this shot occurred at 340 msec). Fig. 2 shows a plot of the innermost four channels of GPC data, time expanded about $t = 115$ msec. Two things which should be emphasized are that the electron temperature (T_e) was hollow and the fluctuation frequency was ~ 3 kHz. Similar temperature fluctuations were observed on the GPC2 fast channels, but the raw signals

were noisy. It is thus clearer to compare the Fourier-transformed amplitudes. The Fourier-transformed amplitudes at ~ 3 kHz of the two combined GPCs (GPC and GPC2) clearly show that the fluctuations were localized within 2 cm ($\Delta\rho \sim 0.1$) plotted in Fig. 3. Each point in Fig. 3 is chosen from the combined data set, whose positions are also referenced to other diagnostics; before, during and after the fluctuations (the time windows over which data was averaged are illustrated as shaded regions of Fig. 2). Meanwhile, a coherent frequency at 3.2 kHz was observed on the magnetics as shown by the Fourier transformed amplitudes in Fig. 4.

From the magnetics, the toroidal mode number was identified as $n = 1$. The MHD activity is found to rotate in the direction opposite to the plasma current I_p . This direction is equivalent to the ion diamagnetic drift direction, since we conjecture that the magnetic fluctuations originate from the same region where the electron temperature fluctuations are observed. As a note, the usual counter- I_p direction is equivalent to the electron diamagnetic drift direction in standard ($\mathbf{B} \times \nabla\mathbf{B}$ towards X-point) magnetic field operation because the pressure gradient is monotonic and negative with respect to the radial coordinate ($dp/dr < 0$). However, for an inverted pressure profile ($dp/dr > 0$), the counter- I_p direction becomes equivalent to the ion diamagnetic drift direction. The determination of the poloidal mode number (m) is uncertain, but when we assumed that the core plasma flux surfaces are nearly circular ($\kappa \sim 1.26$), either $m = 5$ or $m = 6$ was found to be likely.

The electron density was determined from the visible Bremsstrahlung, which has been successfully cross-checked with other density measurements, such as Thomson scattering and reflectometry. Based on this diagnostic, the density profile was found to be weakly decreasing with R in the core, as shown in Fig. 5. Assuming that the equilibration time between electrons and ions was short we estimated $T_i(r)/T_e(r) \approx 0.9$. Thus, the total pressure profile, as well as the electron pressure profile, was found to be hollow, as shown in Fig. 5. An alternative estimate of the $T_i(r)$ profile is discussed in Sec. IV.

III. Theoretical interpretation

A. Equilibrium

Using the pressure profile as an additional constraint to the EFIT program, an equilibrium with reversed magnetic shear was constructed with $q(0) \gg 1$. Fig. 6 shows the EFIT-reconstructed pressure profile with the input pressure constraints indicated. The associated q -profile is also shown. Comparison with Fig. 3 shows that the localized fluctuations were observed near the inner $q = 5$ rational surface ($\rho \sim 0.22$). Here ρ is a normalized minor radius defined as $\sqrt{V(\psi)/V_{tot}}$, where $V(\psi)$ denotes the plasma volume enclosed by a flux surface and V_{tot} the whole plasma volume. Thus, the case of $m/n = 5/1$ is found to be more likely than that of $m/n = 6/1$.

B. Ideal MHD stability theory

The MHD stability calculations using the MARS code¹⁵ and a quasi 1-D model predict a localized MHD mode to be ideally unstable, as described in the following subsections.

1. 2-D Toroidal Ideal and Resistive MHD Simulations

Instability studies using the MARS code (with toroidal mode number, $n = 1$) show two modes predicted to be unstable. Fig. 7 shows the scaling of their growth rates, γ , with Lundquist number, $S = \tau_R \omega_A$, where τ_R is the current diffusion time [$\tau_R = \mu_0 a^2 / \eta$, where μ_0 is the vacuum permeability ($4\pi \times 10^{-7}$ H/m), a scale length, and η resistivity], and $\omega_A = B_0 / R(\mu_0 \rho)^{1/2}$ (R is the major radius and ρ mass density). S_0 is the Lundquist number S at $r=0$. One mode is the double tearing mode,¹³ for which $\gamma \sim S_0^{-3/5}$. The other, which has the higher growth rate at the experimental value of S_0 , is identified as an ideal-unstable mode by the observation that the growth rate [$\gamma \sim \gamma_I \sim 1.0 \times 10^{-3} \omega_A$, where γ_I is ideal growth rate] becomes constant at high S_0 . Fig. 8 shows the radial structure of the pressure fluctuations (δp) and its poloidal harmonic content. The peak is located at the inner $q = 5$ rational surface ($\rho \sim 0.22$). The experimental perturbation in Fig. 3 agrees reasonably well with the radial structure of the MARS code.

Evaluation of the exact Mercier² stability criterion,

$$D_M - 1/4 < 0, \quad (1)$$

which is performed by the MARS code on each flux surface, reveals that this criterion is violated across a substantial region of the plasma core where the pressure gradient is reversed ($dp/dr > 0$). Near the magnetic axis, if the magnetic surfaces are approximately circular, D_M takes the form:

$$D_M = \frac{-2\mu_0 r p'(1 - q^2)}{B^2 s^2} \quad (2)$$

with the shear $s \equiv r q'/q$ and primes representing radial derivatives. The key factors contributing to violation of the Mercier criterion in the core of C-Mod are the large values of q ($q^2 > 20$), the moderate shear, and the reverse pressure gradient.

It is therefore natural to identify the observed fluctuations with an $n = 1$ and dominantly $m = 5$ Mercier instability. The poloidal harmonic content (in Fig. 8) provides further support, since a feature of Mercier analysis is a weak ‘ballooning’ content in which all harmonics are centered on the same rational surface, in this case $q = 5$. This feature distinguishes Mercier instability from true ballooning instabilities in which each poloidal harmonic, m , is centered on its own rational surface at $m = nq$, leading to a more radially extended eigenmode structure. However, the identification of highly localized temperature fluctuations in the C-Mod core with an instability of Mercier type raises the question of whether, since the Mercier stability criterion is violated over an extended region, other Mercier modes were also present and if not, why not. We return to this question later.

2. Quasi 1-D Ideal MHD analysis

A surprisingly accurate replication of the fully 2-D MARS results was obtained by solving a 1 - D eigenmode equation for $\xi_r^{(m=5)}$, of the form¹⁶:

$$\frac{d}{dr} \left\{ r^3 A \frac{d\xi}{dr} \right\} - r\xi(m^2 - 1)A + r\xi D_M s^2 = 0 \quad (3)$$

with

$$A = \left(\frac{m - nq}{q}\right)^2 + \frac{\gamma^2}{\omega_A^2}(1 + q^2 f_+ + q^2 f_-) \quad (4)$$

$$f_{\pm} = \frac{\omega_s^2}{\gamma^2 + \omega_s^2(m \pm 1 - nq)^2} \quad (5)$$

$$\omega_s = C_s/Rq, \quad C_s^2 = \frac{5}{3} \frac{p}{\rho} \quad (6)$$

This, apparently cylindrical, equation contains two important toroidal effects:

- (i) In $D_M s^2 \simeq -2r\mu_0 p'(1 - q^2)/B^2$, the q^2 term represents both the effect of average toroidal curvature and the effect of ‘weak ballooning’ (the presence of the small sideband harmonics visible in the MARS eigenfunction in Fig. 8).
- (ii) The inertial enhancement factor, $[1 + q^2(f_+ + f_-)]$, represents inertial contributions from large sideband ($m = 4$ and $m = 6$) longitudinal displacements (ξ_{\parallel}), and also the effects of adiabatic compression at finite growth rate γ . For sub-sonic growth rates it reduces to the familiar form $(1 + 2q^2)$.

Solution of Eq. 3, with $q(r)$ and $p(r)$ profiles similar to those used in the MARS simulations and the value of D_M taken from MARS, yields $\gamma \sim 0.95 \times 10^{-3} \omega_A$, within 5% of the value ($\gamma_I \sim 1.0 \times 10^{-3} \omega_A$) obtained from the MARS code. The corresponding eigenfunction is shown in Fig. 9. These Mercier growth rates are in fact subsonic.

C. The Effect of Finite Ion Larmor Radius (FLR) Stabilization

The FLR modified eigenvalue^{8,17} can immediately be obtained from the ideal MHD result, calculated by e.g. the MARS code, by solving the dispersion relation,

$$\omega(\omega - \omega_{*i}) + \gamma_I^2 = 0, \quad (7)$$

where γ_I is the ideal MHD growth rate, ω is the complex eigenfrequency, and $\omega_{*i} = \frac{nq}{n_e e B r} \frac{dp_i}{dr}$ (assumed constant). For a weak instability, inertia is only important close to the resonant magnetic surface so that only $\omega_{*i}(r = r_s)$ is

required, where r_s is the resonant surface location. The result is a pair of modes with $\omega = \omega_{\pm}$ where,

$$\omega_{\pm} = \frac{\omega_{*i}}{2} \pm \sqrt{\frac{\omega_{*i}^2}{4} - \gamma_I^2} \quad (8)$$

Thus, when

$$\gamma_I < \frac{\omega_{*i}}{2}, \quad (9)$$

the ideal MHD solutions are replaced by a pair of marginally stable oscillatory modes with frequencies in the range $[0, \omega_{*i}]$, ie within the diamagnetic gap in the Alfvén continuum.

Surprisingly, for an $n = 1$ ideal mode, when we evaluate ω_{*i} for the core plasma conditions in the Alcator C-Mod discharge, we find that inequality 9 is satisfied and that the ideal $n = 1$ Mercier mode is FLR stabilized. In fact, $\omega_{*i}/2 \sim 2.9 \times 10^4$, while $\gamma_I \sim 1.5 \times 10^4$ [rad/sec]. It is well known,^{18–20} however, that FLR stabilization is not robust. Addition of any plasma dissipation or Landau resonance results in destabilization of one of the oscillatory modes and damping of the other. Which mode is damped and which destabilized depends on the precise nature of the dissipation. In the context of a two fluid analysis of internal kink modes, Porcelli and Migliuolo¹⁸ showed that with the addition of resistivity the ω_- solution is destabilized and the ω_+ solution damped, while perpendicular ion viscosity has the reverse effect. Lakhin and Mikhailovskii¹⁹ have found that longitudinal neo-classical viscosity is similar to perpendicular viscosity in driving ω_+ and damping ω_- .

The task is therefore to identify which dissipative effect is dominant in any given situation. For the conditions of the C-Mod discharges under consideration we have evaluated the following characteristic frequencies: electron collision frequency, ν_e ; ion collision frequency, ν_{ii} ; ion diamagnetic frequency, ω_{*i} , which we take to be roughly equivalent to the mode frequency ω_+ ; thermal ion transit frequency, $\omega_{ti} = \sqrt{2T_i/m_i}/Rq$; and Alfvén transit frequency, $\gamma_A (\equiv \omega_A/q)$. These are listed in Table 1.

From these results we conclude that: (i) electrons are collisional ($\nu_e \gg \omega_{\pm}$); (ii) ions are collisionless ($\nu_{ii} \ll \omega_+$); and (iii) an oscillatory mode for which $\omega \sim \omega_{*i}$ is strongly resonant with passing ions of thermal energy, $\omega \sim \omega_{ti}$.

Ion Landau damping is, therefore, likely to be the dominant form of dissipation for the upper of the two FLR stabilized gap modes, so we examine the relevant kinetic theory in the next section.

D. Kinetic Theory of Mercier modes and the effect of Ion Landau Damping

The relevant ‘inertial layer’ theory for low frequency modes in the presence of ion Landau damping has been developed in a number of papers.^{20–22} Solving the drift kinetic equation for the perturbed ion distribution function one finds that this contains the two sideband harmonics with $m' = m \pm 1$, which are strongly Landau resonant. Parallel ion dynamics is also affected by an electrostatic component in the parallel electric field, so the analysis requires a consistent solution of the quasi-neutrality condition to determine this electric field. The resulting dispersion relation, Eq. (21) of Ref.22, can be written in the form:

$$\omega(\omega - \omega_{*i}) + q^2 \omega \omega_{ti} \left[\left(1 - \frac{\omega_{*ni}}{\omega}\right) F\left(\frac{\omega}{\omega_{ti}}\right) - \frac{\omega_{*ni} \eta_i}{\omega} G\left(\frac{\omega}{\omega_{ti}}\right) - \frac{N^2\left(\frac{\omega}{\omega_{ti}}\right)}{D\left(\frac{\omega}{\omega_{ti}}\right)} \right] + \gamma_I^2 (1 + 2q^2) = 0 \quad (10)$$

where,

$$F(x) = x\left(x^2 + \frac{3}{2}\right) + \left(x^4 + x^2 + \frac{1}{2}\right)Z(x) \quad (11)$$

$$G(x) = x(x^4 + x^2 + 2) + \left(x^6 + \frac{x^4}{2} + x^2 + \frac{3}{4}\right)Z(x) \quad (12)$$

$$N(x) = \left(1 - \frac{\omega_{*ni}}{\omega}\right) \left[x + \left(x^2 + \frac{1}{2}\right)Z(x)\right] \quad (13)$$

$$D(x) = \left(\frac{1}{x}\right)\left(1 + \frac{1}{\tau}\right) + \left(1 - \frac{\omega_{*ni}}{\omega}\right)Z(x) - \frac{\omega_{*ni} \eta_i}{\omega} \left[x\left(x^2 + \frac{1}{2}\right) + \left(x^4 + \frac{1}{4}\right)Z(x)\right] \quad (14)$$

with $\tau = T_e/T_i$, $\omega_{*n_i} = \frac{nqT_i}{n_i e B r} \frac{dn_i}{dr}$, $\eta_i = d \ln T_i / d \ln n_i$ and $Z(x)$ the plasma dispersion function. Eq. 10 has been solved, with parameter values representing C-Mod conditions ($\omega_{*i}/\omega_{ti} = 0.71$, $\eta_i \sim -2$), and by varying the ideal MHD growth rate (γ_I/ω_{*i}) over the range $[0, 0.7]$, which spans the value

found by the MARS code, $\gamma_I/\omega_{*i}=0.22$. An unstable kinetic Mercier mode is found throughout this range. Figs. 10 and 11 show the growth rate, γ/ω_{*i} , and frequency, ω/ω_{*i} , in this range. For the C-Mod conditions, $\gamma/\omega_{*i}=0.27$ and $\omega/\omega_{*i}=1.34$. This frequency is calculated in the reference frame of the $\mathbf{E} \times \mathbf{B}$ drift. Thus, in the laboratory frame, the mode frequency, obtained by Doppler shifting, is given by

$$\omega = 1.34\omega_{*i} + \omega_E, \quad (15)$$

where ω_E is the $\mathbf{E} \times \mathbf{B}$ drift frequency. To compare with the observed frequency, $f \sim 3.2$ kHz, we first assume that there is no bulk rotation in the plasma core, so that

$$\Omega_{plasma} \sim \omega_{*i}(1 + \frac{a\eta_i}{1 + \eta_i}) + \omega_E \sim 0, \quad (16)$$

where a is a neoclassical coefficient with opposite signs in the banana and plateau regimes. For C-Mod conditions we estimate $a \sim -1/2$. Thus, using Eq. 16 and $\eta_i \sim -2$, we obtain $\omega \sim 1.34\omega_{*i}$, corresponding to frequency $f_{KM} \sim 12$ kHz (f_{KM} is the kinetic Mercier mode frequency). Considering that X-ray spectroscopy²³ during current ramp in other C-Mod ohmic plasmas shows that heavy impurities have toroidal velocities as large as 50 km/sec (corresponding to a toroidal rotation frequency $f_{rot} \sim 12$ kHz) in the counter- I_p direction, the assumption of stationary bulk ions is open to question, even though, as discussed in Ref. 24, the rotation of the heavy impurity ions can differ significantly from that of the bulk ions. These uncertainties are compounded by the fact that ω_{*i} and the neoclassical corrections to the equilibrium toroidal rotation depend on the ion temperature profile, which is itself very uncertain. We return to this point in Sec.IV and conclude that there is not sufficient data to make a meaningful comparison of the observed mode frequency with theoretical prediction.

As noted earlier, the Mercier stability criterion was found to be violated across a substantial region of the plasma core in C-Mod, where the pressure gradient was reversed. This raises the question of what other ‘Mercier-type’ instabilities are predicted to be unstable theoretically. In this connection we first note that to have a Mercier instability centered at, e.g. $q = 5.1$, requires $m = 51$ and $n = 10$ and that the localization of the plasma displacement, ξ_r , for such a mode is determined from Eq. (3), with:

$$\xi_r \sim r^{50}, \quad \text{for } r < r_s$$

$$\xi_r \sim r^{-52}, \quad \text{for } r > r_s,$$

predicting an exceptionally narrow eigenmode. In addition, the predicted mode frequency, with $\omega \sim \omega_{*i}$, would be so high that ion resonance effects would be negligible. Therefore, other forms of dissipation must determine the stability of such modes. Thus only low order resonances with $q = 5/1, 9/2, 4/1, \dots$ are likely to result in kinetic Mercier instabilities of the type discussed here. However, for the EFIT equilibrium under consideration, the $q = 9/2, 4/1$ resonances lie in the Mercier stable region, with $dp/dr < 0$.

IV. Uncertainties in the equilibrium reconstruction and their consequences

Although the spatial dependence of the density and the electron temperature are quite accurately known, there is no direct observational data for the ion temperature. Because of the relatively low core temperature ($T_e \sim 600\text{eV}$), in constructing the EFIT equilibrium, a strong coupling approximation [$T_i(r) \sim T_e(r)$] was employed in estimating the ion temperature. As an alternative to the strong coupling approximation we have calculated $T_i(r)$ from a 1-D time dependent diffusion equation, in which neoclassical ion thermal conduction (with the Chang-Hinton²⁷ expression for χ) is balanced by classical electron-ion equilibration, and the known $T_e(r)$ is ramped in time on the experimental time scale of about 100msec. The $T_i(r)$ obtained from this calculation and shown in Fig.12 is only weakly non-monotonic in the plasma core, with the result that the total pressure gradient is somewhat smaller than in the strong coupling case. To investigate the consequences of the experimental uncertainties in the ion pressure, and in the total pressure, we have generated a second EFIT equilibrium using this slightly different pressure data, and investigated its MHD stability properties with the MARS code and its kinetic stability (with diamagnetic and ion Landau resonance modifications), by solving Eq. 10. We will refer to this equilibrium as E2 and the original one as E1.

Because the ion temperature gradient in E2 is much smaller than in E1, the Mercier stability parameter D_M (Eq. 2) drops from ~ 0.87 in E1 to a

value of ~ 0.38 in E2. Although E2 is still Mercier unstable, the ideal MHD growth rate is much smaller than in E1; $\gamma_I \sim 6 \times 10^{-5} \omega_A$ in E2 compared to $10^{-3} \omega_A$ in E1. The MARS code, however, indicated that there is a significant resistive enhancement of the ideal growth rate in E2 at the C-Mod relevant value of the Lundquist number, with $\gamma_{cmod} \sim 0.4 \times 10^{-3} \omega_A$. The exceptionally small value of the ideal growth rate for the equilibrium E2 is in qualitative agreement with results from the 1-D “cylindrical” stability code (described in Sec. III) and with the analysis of Kulsrud.²⁸

The ion diamagnetic frequency, ω_{*i} , is also smaller in E2 than in E1 but, because of the even greater reduction in the ideal growth rate, the theoretical prediction that the ideal mode is FLR stabilized remains unchanged. In E2 the oscillatory FLR stabilized Mercier modes have frequencies at the extreme ends of the diamagnetic gap in the Alfvén continuum, with $\omega_- \sim 0$ and $\omega_+ \sim \omega_{*i}$. As discussed before, it is important to investigate the effects of resistivity and inverse ion Landau damping on these stable modes. Repeating the solution of the kinetic dispersion relation, Eq. 10, with $\gamma_I \sim 6 \times 10^{-5} \omega_A$, $\omega_{*i} \sim 1.4 \times 10^{-3} \omega_A$, $\omega_{*i}/\omega_{ti} \sim 0.25$ and $\eta_i \sim -0.45$, we find a Landau driven instability with $\omega \sim 0.6 \omega_{*i}$ and $\gamma \sim 0.1 \omega_{*i}$. The effect of resistivity on the ω_- and ω_+ modes (or equivalently the effect of diamagnetic corrections to the resistive instability found by the MARS code in E2) can also be calculated, and reveals that resistivity also destabilizes the ω_+ mode.

From the foregoing analysis we draw the following, rather tentative, conclusions:

- (i) Taking account of uncertainties in the ion temperature, the equilibrium during current ramp in the C-Mod discharge under consideration appears to have violated the Mercier stability criterion (although it should be noted that a 25% increase in the shear at the $q=5$ surface would be sufficient to reduce D_M to the marginal value of $1/4$ in E2).
- (ii) The corresponding ideal MHD growth rates are sufficiently weak that diamagnetic effects stabilize the Mercier mode predicted by ideal MHD analysis and computation.
- (iii) Collisionless ion dynamics, or finite resistivity can then be shown to be responsible for driving a residual mode with $\omega \sim \omega_{*i}$. In the case of equilibrium E1 it is clear that inverse ion Landau damping is effective in doing this. For the alternative equilibrium, E2, both inverse ion damping and resistivity drive this branch of the dispersion relation. But the resonant ion analysis is breaking down in this case because the resonant ions have subthermal lon-

gitudinal velocities, and the slab-like analysis of Zonca, Chen and Santoro does not take account of magnetic trapping. In this case collisional trapped ion dissipation (see for example Mikhailovskii *et al.*²⁰) may provide a similar destabilizing mechanism.

V. Discussion and Conclusions

Detailed theoretical studies, with both an MHD code and a collisionless ion kinetic analysis, have led to the possible identification of the localized temperature fluctuations in some reversed shear discharges in Alcator C-Mod as $n = 1$ FLR modified kinetic Mercier instabilities. The C-Mod observations may therefore be the first observation of a Mercier instability in tokamaks. They indicate that, at least for $m = 5$, the instability seems to be relatively benign, possibly because of its localized nature. We note that the kinetic Mercier instability has a substantial growth rate as $\gamma_I \rightarrow 0$, i.e as the Mercier criterion becomes marginally satisfied.

We have seen very similar localized MHD phenomena in several discharges, but in some cases the pressure gradients were not as large as the case discussed here. Some of these equilibria may not be ideal MHD unstable. When the Mercier criterion is not violated, $0 < D_M \sim D_R < 1/4$ ($D_R < 0$ is a stability criterion for resistive interchange mode²⁵), there are two possible theoretical explanations for such localized MHD activity; an ion Landau driven mode and a resistive interchange mode. Within this range of parameters the MARS code predicts instability of the resistive interchange mode with growth rates $\sim O(10^{-3}\omega_A)$. Observations of localized fluctuations in ASDEX-Upgrade have recently been interpreted (with the aid of the CASTOR code) in terms of localized resistive interchange instability.²⁶ The relevant ASDEX discharges, with reversed shear and hollow pressure profiles, are similar to those discussed here, but no information on the magnitude of $D_M \sim D_R$ was given. As discussed in Sec.IV distinguishing the kinetic Mercier mode from the resistive interchange mode is difficult. In the resistive MHD calculations (eg in the MARS and CASTOR codes), diamagnetic and ion Landau damping effects are neglected. In the analysis of Secs. III. D, IV. [the solution of Eq. 10], we have neglected the effect of resistivity on the kinetic Mercier mode. In a fully kinetic treatment the mode frequencies of

the resistive interchange mode and the Landau driven Mercier mode may be distinct, but identifying the observed fluctuations by comparing their fluctuation frequency with the theoretical mode frequencies is impossible because of uncertainties in both the ion temperature gradient and the radial electric field.

We conclude that violation of the Mercier criterion at a low order rational magnetic surface in C-Mod does result in instability, irrespective of diamagnetic effects, and that the localized temperature fluctuations in the core of C-Mod can be attributed to a modified Mercier instability.

Acknowledgements

The authors would like to thank the Alcator C-Mod group for the successful operation. This work has been supported by USDOE Cooperative Agreement DE-FC02-99ER54512.

References

- ¹I. H. Hutchinson, R. Boivin, F. Bombarda *et al.*, Phys. Plasmas **1** 1511 (1994)
- ²C. Mercier, Nucl. Fusion **1** 47 (1960)
- ³J. N. Talmadge and W. A. Cooper, Phys. Plasmas **3** 3713 (1996)
- ⁴K. Ichiguchi, Plasma Phys. and Controlled Fusion **39** 1805 (1997)
- ⁵T. Ozeki, M. Azumi, S. Ishida, and T. Fujita, Plasma Phys. and Controlled Fusion **40** 871 (1998)
- ⁶M. S. Chance, C. Kessel, and S. C. Jardin, Plasma Phys. and Controlled Fusion **41** 1379 (1999)
- ⁷T. Ozeki, M. Azumi, S. Ishida, and T. Fujita, Plasma Phys. and Controlled Fusion **41** 1429 (1999)
- ⁸K. V. Roberts and J. B. Taylor, Phys. Rev. Lett. **8** 197 (1962)
- ⁹G. Ara, B. Basu and B. Coppi, Annals of Phys. **112** 1978 443
- ¹⁰J. W. Connor, W. M. Tang, L. Allen, Nucl. Fusion **24** 1023 (1984)
- ¹¹W. M. Tang, R. L. Dewar and J. Manickam, Nucl. Fusion **22** 1079 (1982)
- ¹²L. L. Lao, J. R. Ferron, R. J. Groebner, W. Howl, H. St. John, E. J. Strait and T. S. Taylor, Nucl. Fusion **30** 1035 (1990)
- ¹³Y. In, J. J. Ramos, A. E. Hubbard, I. H. Hutchinson, M. Porkolab, J. Snipes, S. Wolfe, A. Bondeson, Nucl. Fusion **40** 1463 (2000)
- ¹⁴Z. Chang, W. Park, E. D. Fredrickson *et al.*, Phys. Rev. Lett. **77** 3553 (1996)
- ¹⁵A. Bondeson, G. Vlad and H. Lütjens, Phys. Fluids B**4** 1889 (1992)
- ¹⁶C. Wahlberg, Journal of Plas. Phys. **62** 165 (1999)

- ¹⁷M. N. Rosenbluth, N. A. Krall and N. Rostoker, Nucl Fus Suppl. **1** 143 (1962)
- ¹⁸F. Porcelli and S. Migliuolo, Phys. Fluids **29** 1741 (1986)
- ¹⁹V. P. Lakhin and A. B. Mikhailovskii, Physics Letts A. **191** 162 (1994)
- ²⁰A. B. Mikhailovskii, S. V. Nazarenko and A. P. Churikov, Sov. J Plasma Phys. **15**, 19 (1989)
- ²¹F. Romanelli, L. Chen and R. B. White, Nucl. Fusion **31** 631 (1991)
- ²²F. Zonca, L. Chen and R. A. Santoro, Plasma Phys. and Controlled Fusion **38** 2011 (1996)
- ²³J. E. Rice, E. S. Marmor, F. Bombarda, L. Qu, Nucl. Fusion **37** 421 (1997)
- ²⁴Y. B. Kim, P. H. Diamond and R. J. Groebner, Phys. Fluids B**3** 2050 (1991)
- ²⁵R. J. Glasser, J. M. Greene and J. L. Johnson, Phys. Fluids **19** 567 (1976)
- ²⁶S. Günter, A. Gude, H. R. Koslowski, M. Maraschek, S. D. Pinches, S. Sesnic, Q. Yu, ASDEX Upgrade Team, Nucl. Fusion **39**, special issue, (1999) 1793
- ²⁷C. S. Chang and F. L. Hinton, Phys. Fluids **25** 1493 (1982)
- ²⁸R. M. Kulsrud, Phys. Fluids **6** 910 (1963)

Tables

TABLE I. Characteristic frequencies

Figures

FIG. 1. MHD activity during a current ramp discharge. Near $t=115$ msec, highly localized MHD fluctuations were observed on the second channel and then sawtooth-like crashes followed later.

FIG. 2. Highly localized MHD activity on the innermost four GPC channels. Note that the MHD is extraordinarily localized on the second channel and that the temperature profile was hollow; near $t=115$ msec, $T_e(\text{Ch } 1)=0.61 < T_e(\text{Ch } 2)=0.77 < T_e(\text{Ch } 3)=0.88 > T_e(\text{Ch } 4)=0.78$ in keV units. See also the electron temperature profile in Fig. 5. Each shaded area represents the time bin for comparison with magnetics; ‘before’, ‘during’ and ‘after’ this fluctuation.

FIG. 3. Fourier-transformed fluctuation amplitudes at ~ 3 kHz of the combined dataset of GPC and GPC2. The amplitudes are normalized with respect to the highly peaked GPC channel amplitude. The amplitudes during the localized MHD activity are contrasted with those before and after the event. Later, the comparison with the MARS results corroborates that the event was due to ideal interchange mode.

FIG. 4. Fourier-transformed magnetic signals before, during and after the localized MHD activity. The coherent frequency near 3.2 kHz is dominant during the event. Each time bin of ‘before’, ‘during’ and ‘after’ is defined in Fig. 2.

FIG. 5. Electron temperature (T_e), density (n_e), pressure (p_e) and total pressure ($p = p_i + p_e$) profiles. Note that the electron temperature is hollow, while the density is weakly decreasing. The total pressure is also hollow. Each circle represents one of the combined locations of GPC and GPC2. The dashed rectangle is the location of the localized MHD event from the combined data set.

FIG. 6. Safety factor and pressure profiles. The asterisks (*) represent pressure inputs to the EFIT reconstruction, while the solid curve is the EFIT output. Note the inner $q = 5$ surface is located in the inverted pressure gradient region ($dp/dr > 0$).

FIG. 7. Growth rates vs resistivity using the MARS code. The Alcator C-Mod case is circled. As the resistivity decreases, the growth rates become independent of it, which is characteristic of ideal MHD mode. The dashed (solid) line is the theoretical growth rate of the resistive interchange (multiple tearing) mode.

FIG. 8. $n = 1$ ideal interchange mode. Near the inner $q = 5$ rational surface, the fluctuations are highly localized. Each symbol represents a poloidal mode component. The dash-dot curve delineates the predicted total pressure fluctuations (δp), with $S_0 = 1.25 \times 10^7$ and $\gamma\tau_A \sim 1.2 \times 10^{-3}$, where γ is growth rate [rad/sec] and τ_A is the Alfvén time $\sim 8 \times 10^{-8}$ sec.

FIG. 9. Eigenfunction based on a quasi 1-D model. The comparison with Fig. 8 reveals the applicability of the quasi 1-D model.

FIG. 10. Growth rates, $\frac{\gamma}{\omega_{*i}}$. The solid curve is the predicted growth rate from solving Eq. 10. It is based on retaining all contributions from ideal MHD stability, FLR effects, and ion Landau damping dissipation. The dashed (dash-dot) curve results from ideal MHD with (without) the FLR stabilization effect. Note that the gap mode is located between the ideal boundary ($\delta W \equiv 0$) and FLR stabilized boundary.

FIG. 11. Predicted frequency (ω/ω_{*i}) in the reference frame of the $\mathbf{E} \times \mathbf{B}$ drift.

FIG. 12. Ion temperature profile $T_i(r)$ calculated from time dependent neo-classical diffusion equation with Chang-Hinton χ_\perp and measured $T_e(r)$, which is also shown.

Table 1: Characteristic frequencies

Notation	Frequency [rad/sec]
γ_A	2.5×10^6
γ_I	1.3×10^4
ω_{*i}	5.8×10^4
ω_{ti}	8.2×10^4
ν_{ii}	2.7×10^3
ν_e	2.3×10^5

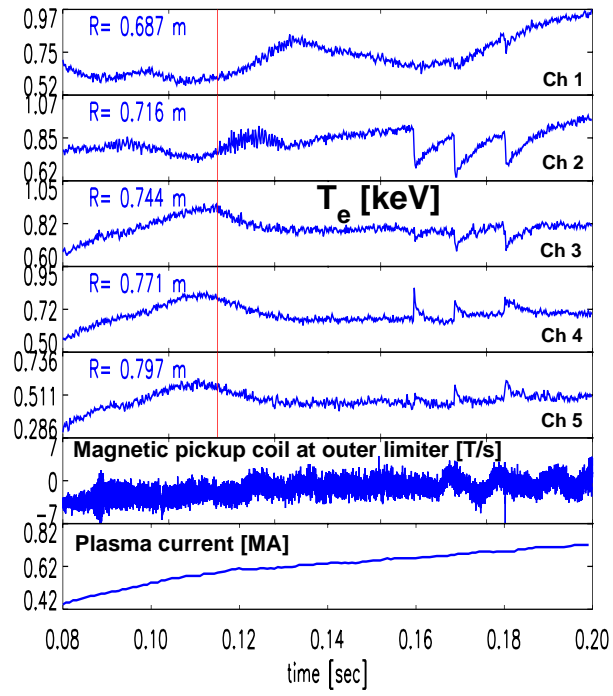


Figure 1:

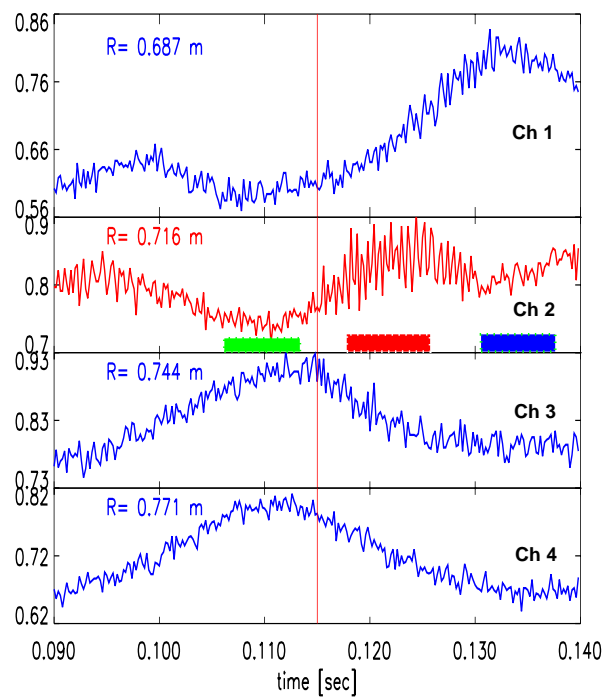


Figure 2:

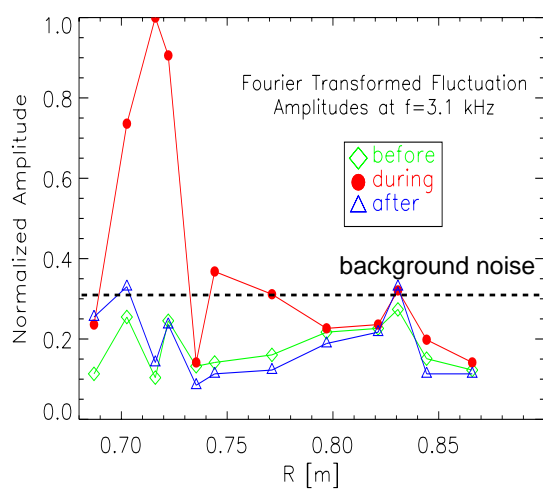


Figure 3:

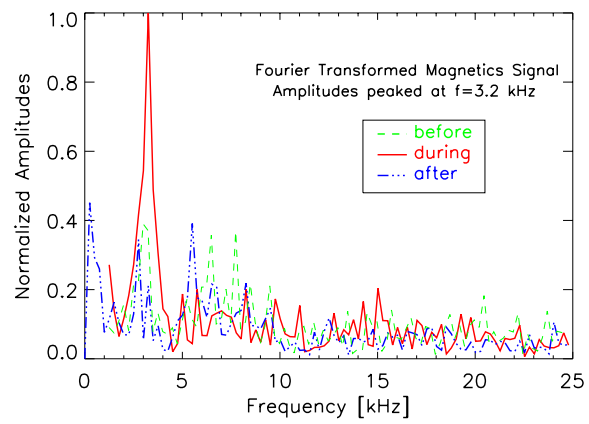


Figure 4:

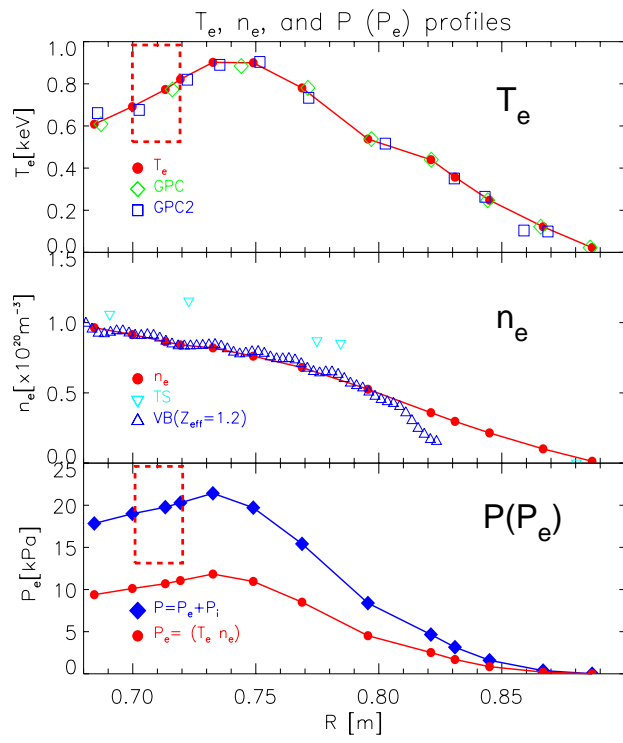


Figure 5:

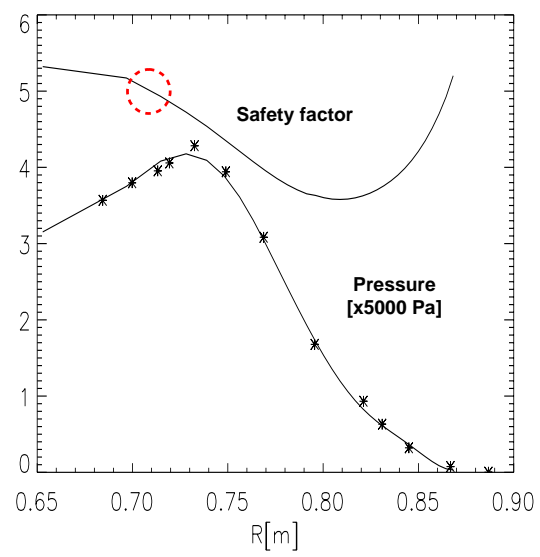


Figure 6:

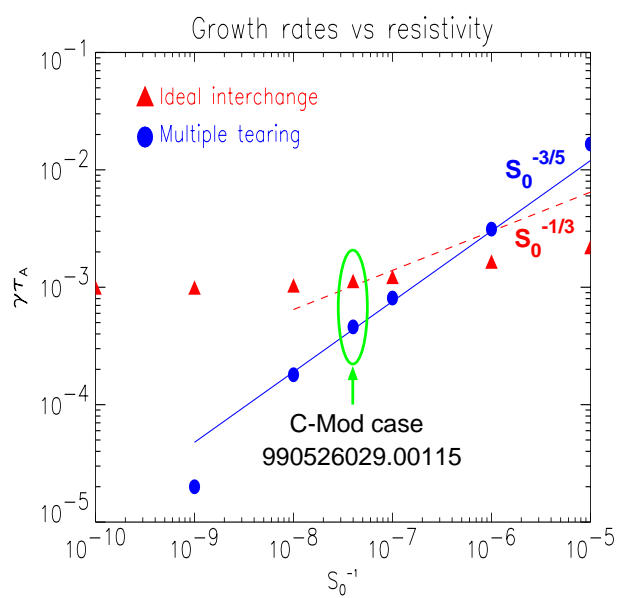


Figure 7:

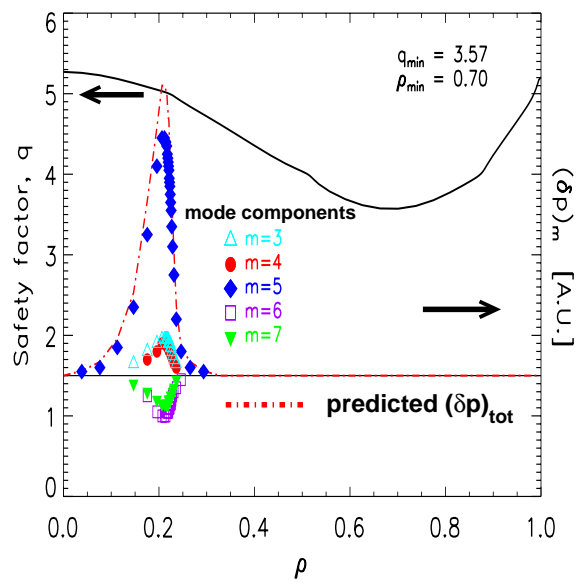


Figure 8:

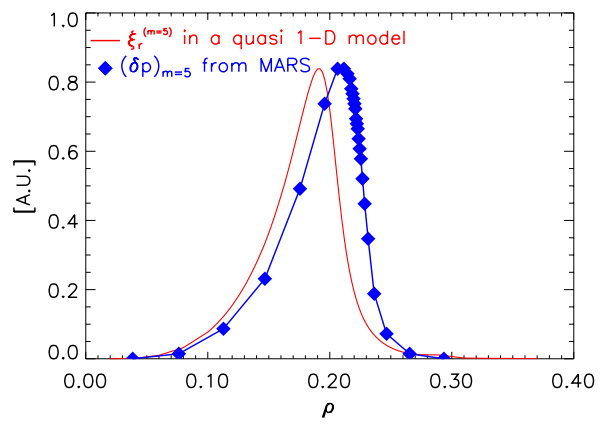


Figure 9:

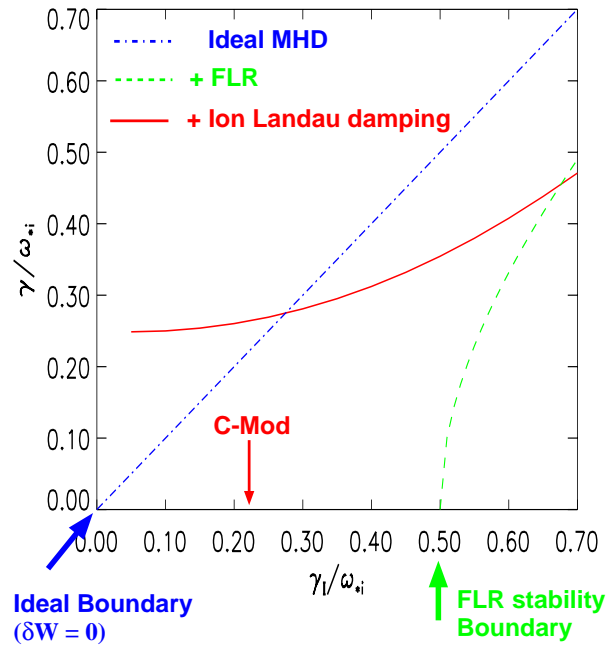


Figure 10:

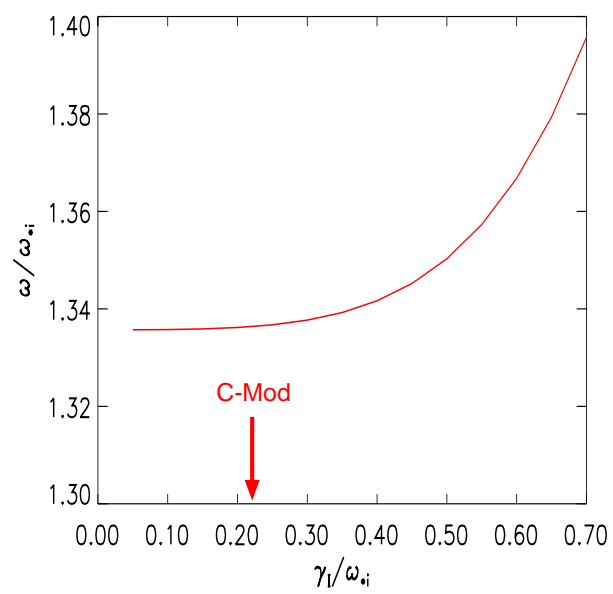


Figure 11:

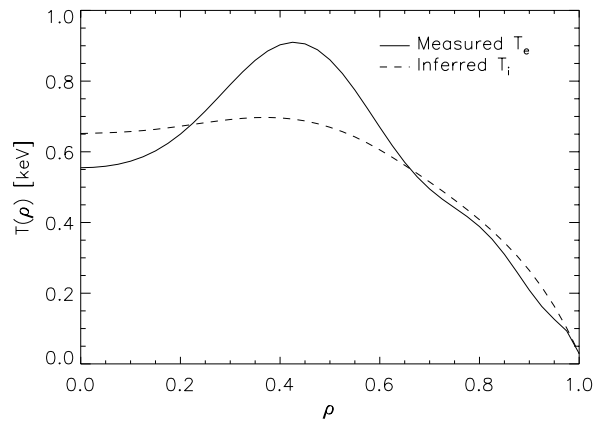


Figure 12: